On the dynamic analysis of a novel snake robot: preliminary results

Giuseppe Quaglia[1], Paride Cavallone[1], Basilio Lenzo[2]

[1] *Politecnico di Torino, Italy, e-mail: giuseppe.quaglia@polito.it paride.cavallone@polito.it,*

[2] *Sheffield Hallam University,UK, e-mail: basilio.lenzo@shu.ac.uk*

Abstract. In recent years, modular robotics has become of great interest in the robotics community. Among them, snake robots are among the most flexible and versatile type of mobile robots, well-suited to a large number of applications, such as exploration and inspection tasks, participation to search and rescue missions etc. The present paper investigates the design of a novel snake robot, named Rese_Q01, currently being designed at Politecnico di Torino. In order to characterise the dynamic behaviour of the robot, a simple vehicle dynamics model is developed and basic simulations are carried out for a first implementation of a unit consisting of two modules. Preliminary results show the influence of the robot velocity on the trajectory curvature radius, as well as the effect of different ground/tire friction conditions. This analysis is the first step in order to develop effective control strategies for robot trajectories.

Keywords: Mobile robot, Vehicle dynamics, Snake robot, Rese_Q01.

1 Introduction

In recent years, the service robotic is reaching a higher importance in the robotics community [1]. Generally, service robot means "semi-automatic or automatic robot that helps with its services the human comfort; the manufactory field is exluded" [1]. Mobile robots are meaningful examples of service robots, that are implementing novel key technologies. Mobile robots can be classified by the environment in which they travel, for example UGVs (Unmanned Ground Vehicles) [12], UAVs (Unmanned Aerial Vehicles) [10] and AUVs (Autonomous Underwater Vehicles) [2], or by the device that they use to move as legged robot [11,3], wheeled robot [19,3] and tracked robot [3], or by the work that they do as transportation, mapping, cleaning, assistance and so forth.

Rese_Q01 is a novel mobile ground tracked modular robot [13] that works in dangerous areas as damaged building by explosion, earthquakes in order to explore to find victims, to provide images and other data on the inspected area. Rese_Q01 is composed by five modules, interconnected by motorized joints with three degrees of freedom. The innovative characteristcs of Rese_Q01 is the decision to avoid dividing the robot in two subsystems namely the mobile platform and the robotic arm. The developed robot can use some modules as robotic arm and other modules with the platform function. The robot can employ the snake-like architecture [20] in the motion phase and the robotic arm configuration when the operational function is required, as shown in Fig. 1.

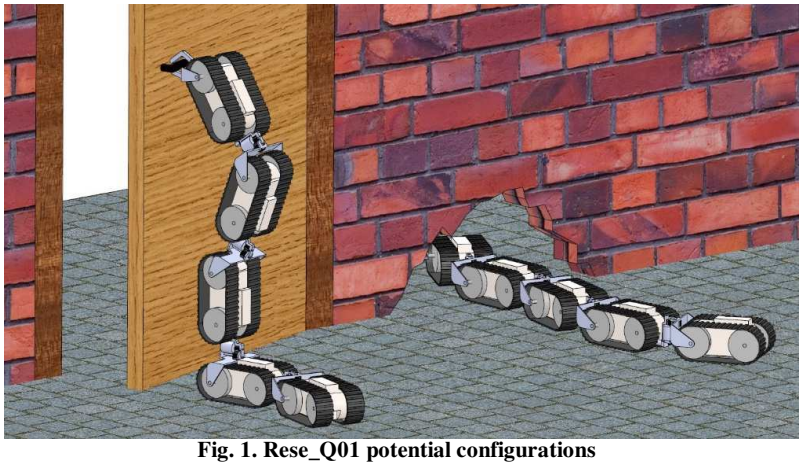

Fig. 1. Rese_Q01 potential configurations

In order to develop trajectory control of the Rese_Q01 robot, effective models of the robot must be defined, analized and discussed. Each module has some slippage between tracks and contact surface, and the resulting trajectory depends on the local contact conditions and the yaw angle between each module. The final goal is to define proper strategies to define all the yaw angles between modules, in order to get both the desired trajectory and limited energy dissipation due to slippage.

In this paper, a simplified dynamic model of the robot will be implemented, with the purpose of supporting the design team. In each module the contact area is the surface under the tracks, but in order to understand some basic dynamics effects of the design parameters (mass, module width and length, position of the yaw joint between modules) it was decided first to simplify the system assuming a line of contact between a rolling element and the supporting surface. As second step a deeper analisys will be developed, describing also the elastic behaviour of the track and including the dimensions of the contact surface.

The work of this paper is supported by the wide experience of the authors in different fields as mobile robotics [12-14], service robotics [15-16] and vehicle dynamics [5,8,17-18].

2 Dynamic model

The dynamic model of the vehicle-robot described hereafter, and shown in Fig. 2, relies on the following hypotheses and assumptions:

- the robot is made of two modules only, each of them being a roller wheel of radius R and width b, and a connecting joint to the previous/following module;
- each roller angular velocity is constant and equal to ω;
- the mass of each module, m, is uniformly distributed only in each roller, and the frame mass is neglected, whilst the centre of mass of the robot is denoted as C;
- the contact between module and ground is a line, corresponding to the module width, characterized by the constant friction coefficient μ;
- the distribution of normal force per unit length of each roller is constant and equal to $p = {}^{mg}/_{b}$, where g is gravity acceleration (this hyphotesis is valid only within limited dynamic behaviours);
- point O is the connection point between module 1 and module 2;
- point P_1 is the centre of roller 1 contact line, Point P_2 is the centre of roller 2 contact line; the generic length OP_i has magnitude d;
- a reference frame $\mathbf{x_1}$-$\mathbf{y_1}$-$\mathbf{z_1}$ is integral with module 1 and centred in O, this frame is denoted as $\{S_1\}$. Axis $\mathbf{z_1}$ is defined according to the right-hand rule, i.e. it is towards the observer. Unit vectors $\mathbf{i_1}$, $\mathbf{j_1}$ and $\mathbf{k_1}$ are defined accordingly;
- a reference frame $\mathbf{x_2}$-$\mathbf{y_2}$-$\mathbf{z_2}$ is integral with module 2 and centred in O, this frame is denoted as $\{S_2\}$. Axis $\mathbf{z_2}$ is defined according to the right-hand rule, i.e. it is towards the observer. Unit vectors $\mathbf{i_2}$, $\mathbf{j_2}$ and $\mathbf{k_2}$ are defined accordingly;
- simulations are conducted assuming a constant yaw angle between the modules, θ, defined as the angle between axes $\mathbf{x_1}$ and $\mathbf{x_2}$, positive counter-clockwise;
- the overall longitudinal force (with respect to $\{S_1\}$) generated at the roller-road contact of module 1 is $Fx_1\ \mathbf{i_1}$, with an offset $Y_1\mathbf{j_1}$ from P_1. The overall lateral force (with respect to $\{S_1\}$) generated is $Fy_1\mathbf{j_1}$;
- the overall longitudinal force (with respect to $\{S_2\}$) generated at the roller-road contact of module 2 is $Fx_2\ \mathbf{i_2}$, with an offset $Y_2\mathbf{j_1}$ from P_2. The overall lateral force (with respect to $\{S_2\}$) generated is $Fy_2\mathbf{j_2}$;
- the velocity of the centre of mass is denoted as $\boldsymbol{V}$, its components along $\mathbf{i_1}$ and $\mathbf{j_1}$ are u and v. Hence $\boldsymbol{V} = u\mathbf{i_1} + v\mathbf{j_1}$; the yaw velocity of the module, is $\dot{\psi}\boldsymbol{k_1}$;
- in the remainder, a generic quantity x expressed with respect to the reference frame $\{S_i\}$ will be indicated as ${}^{i}(x)$.

This set of hypotheses is justified by the current early stage of the robot design. A large amount of such hypotheses is expected to be dropped as the design phase progresses.

Due to the schematic adopted, ${}^{\mathbf{1}}(\boldsymbol{OP_1}) = [d \quad 0]^T$, ${}^{\mathbf{1}}(\boldsymbol{OP_2}) = [-d\cos\theta \quad d\sin\theta]^T$, ${}^{\mathbf{2}}(\boldsymbol{OP_2}) = [-d \quad 0]^T$. Therefore ${}^{\mathbf{1}}(\boldsymbol{OC}) =$

$\frac{^1(\boldsymbol{OC})+\,^1(\boldsymbol{OC})}{2} = \left[\frac{d}{2}(1-\cos\theta) \quad \frac{d}{2}\sin\theta\right]^T$. The relationships between unit vectors of $\{S_1\}$ and $\{S_2\}$ read $\mathbf{i_1} = \mathbf{i_2}\cos\theta + \mathbf{j_2}\sin\theta$, $\mathbf{j_1} = -\mathbf{i_2}\sin\theta + \mathbf{j_2}\cos\theta$, $\mathbf{k_1} = \mathbf{k_2}$ hence it is easy to obtain $^2(\boldsymbol{OC}) = = \left[-\frac{d}{2}(1-\cos\theta) \quad \frac{d}{2}\sin\theta\right]^T$.

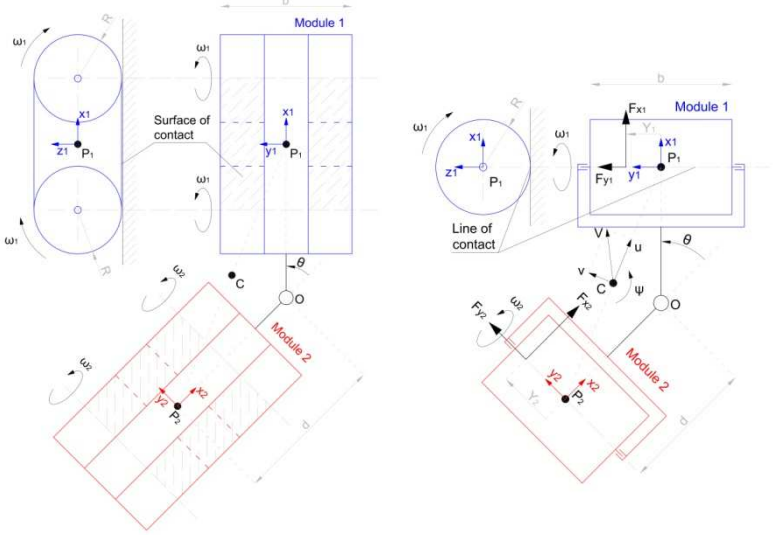

Fig. 2. Schematic of the robot: (left) envisaged configuration, with surface of ocntact; (right) simplified model adopted in this paper, with line of contact

The equilibrium equations, written in $\{S_1\}$, read

$$Fx_1 + Fx_2\cos\theta + Fy_2\sin\theta = Ma_{x1} = M(\dot{u} - v\dot{\psi})$$
$$Fy_1 + Fy_2\cos\theta - Fx_2\sin\theta = Ma_{y1} = M(\dot{v} + u\dot{\psi})$$
$$(Fy_1 - Fy_2)\frac{d}{2}(1+\cos\theta) + Fx_1\left(\frac{d}{2}\sin\theta - Y_1\right) + Fx_2\left(\frac{d}{2}\sin\theta - Y_2\right) = I\ddot{\psi}$$

where the overall mass of the module is $M = 2m$, a_{x1} is the robot acceleration along $\mathbf{i_1}$, a_{y1} is the robot acceleration along $\mathbf{j_1}$, and it is easy to show that they correspond respectively to $\dot{u} - v\dot{\psi}$ and $\dot{v} + u\dot{\psi}$ based on the well-known Poisson's formulae. The moment of inertia I is the sum of the moment of inertia of each module, calculated as the moment of inertia of a cylinder with respect to central diameter, plus an additional contribution considering a translation from P_1 to C for module 1, and from P_2 to C for module 2. Hence

$$I = 2\left(\frac{1}{4}mR^2 + \frac{1}{12}mb^2\right) + m|\boldsymbol{P_1C}|^2 + m|\boldsymbol{P_2C}|^2$$

where

$$|\boldsymbol{P_1C}|^2 = |\boldsymbol{CP_1}|^2 = |\boldsymbol{CO} + \boldsymbol{OP_1}|^2 = |-\boldsymbol{OC} + \boldsymbol{OP_1}|^2$$
$$= \left(-\frac{d}{2}(1-\cos\theta) + d\right)^2 + \left(-\frac{d}{2}\sin\theta\right)^2 = \frac{d^2}{2}(1+\cos\theta)$$

$$|\boldsymbol{P_2C}|^2 = |\boldsymbol{CP_2}|^2 = |\boldsymbol{CO} + \boldsymbol{OP_2}|^2 = |-\boldsymbol{OC} + \boldsymbol{OP_2}|^2$$
$$= \left(\frac{d}{2}(1-\cos\theta) - d\right)^2 + \left(-\frac{d}{2}\sin\theta\right)^2 = \frac{d^2}{2}(1+\cos\theta)$$

Rearranging the equilibrium equations leads to

$$\dot{u} = \frac{Fx_1 + Fx_2\cos\theta + Fy_2\sin\theta}{M} + v\dot{\psi}$$
$$\dot{v} = \frac{Fy_1 + Fy_2\cos\theta - Fx_2\sin\theta}{M} - u\dot{\psi}$$
$$\ddot{\psi} = \frac{(Fy_1 - Fy_2)\frac{d}{2}(1+\cos\theta) + Fx_1\left(\frac{d}{2}\sin\theta - Y_1\right) + Fx_2\left(\frac{d}{2}\sin\theta - Y_2\right)}{I}$$

which can be directly implemented into specifical SW for numerical simulations.

The tangential forces Fx and Fy generated between ground and rollers depend on the sliding velocities of each roller. Fig. 3 shows their generic profile. The longitudinal sliding velocity is calculated as the difference between the longitudinal velocity of each point of the contact line and the relative tangential velocity of the roller, $V_T^r = \omega R$. The velocity of the generic point Q of module 1, $\boldsymbol{V_{Q1}}$, can be calculated based on Rivals' theorem, assuming the robot to be a rigid body

$${}^1\boldsymbol{V_{Q1}} = {}^1\boldsymbol{V_C} + [0 \quad 0 \quad \dot{\psi}]^T \times {}^1\boldsymbol{CQ_1}$$
$$= u\mathbf{i_1} + v\mathbf{j_1} + \dot{\psi}\mathbf{k_1} \times \left[\frac{d}{2}(1+\cos\theta) \quad -\frac{d}{2}\sin\theta + y \quad 0\right]^T$$
$$= \left(u + \dot{\psi}\frac{d}{2}\sin\theta - \dot{\psi}y\right)\mathbf{i_1} + \left(v + \dot{\psi}\frac{d}{2}(1+\cos\theta)\right)\mathbf{j_1}$$

where y is the generic distance from the centre of the module to Q. Similarly,

$${}^1\boldsymbol{V_{Q2}} = {}^1\boldsymbol{V_C} + [0 \quad 0 \quad \dot{\psi}]^T \times {}^1\boldsymbol{CQ_2}$$
$$= u\mathbf{i_1} + v\mathbf{j_1} + \dot{\psi}\mathbf{k_1}$$
$$\times \left[-\frac{d}{2}(1+\cos\theta) + y\sin\theta \quad \frac{d}{2}\sin\theta + y\cos\theta \quad 0\right]^T$$
$$= \left(u - \dot{\psi}\frac{d}{2}\sin\theta - \dot{\psi}y\cos\theta\right)\mathbf{i_1}$$
$$+ \left(v - \dot{\psi}\frac{d}{2}(1+\cos\theta) + \dot{\psi}y\sin\theta\right)\mathbf{j_1}$$

and, recalling the relationship between unit vectors of $\{S_1\}$ and $\{S_2\}$,

$${}^2\boldsymbol{V_{Q2}} = \left(u\cos\theta - v\sin\theta - \dot{\psi}y + \dot{\psi}\frac{d}{2}\sin\theta\right)\mathbf{i_2}$$
$$+ \left(u\sin\theta + v\cos\theta - \dot{\psi}\frac{d}{2}(1+\cos\theta)\right)\mathbf{j_2}$$

The sliding velocities of each module are

$$\Delta\boldsymbol{V_1}(y) = \left(u + \dot{\psi}\frac{d}{2}\sin\theta - \dot{\psi}y - V_T^r\right)\mathbf{i_1} + \left(v + \dot{\psi}\frac{d}{2}(1+\cos\theta)\right)\mathbf{j_1}$$
$$= \Delta V_{1x}\mathbf{i_1} + \Delta V_{1y}\mathbf{j_1}$$

$$\Delta \boldsymbol{V_2}(y) = \left(u\cos\theta - v\sin\theta - \dot{\psi}y + \dot{\psi}\frac{d}{2}\sin\theta - V_T^r\right)\mathbf{i_2} + \left(u\sin\theta + v\cos\theta - \dot{\psi}\frac{d}{2}(1+\cos\theta)\right)\mathbf{j_2} = \Delta V_{2x}\mathbf{i_2} + \Delta V_{2y}\mathbf{j_2}$$

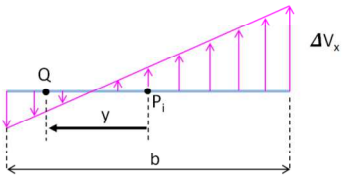

Fig. 3. Generic sliding velocity profile of a roller

The tangential forces generated per unit length, t_1 and t_2 respectively for module 1 and module 2, depend on the slip ratio, defined as the ratio between the sliding velocity and the longitudinal velocity. So

$$t_1(y) = k\frac{|\Delta \boldsymbol{V_1}(y)|}{u_1 - \dot{\psi}y}, \qquad t_1(y) \le \mu p$$
$$t_2(y) = k\frac{|\Delta \boldsymbol{V_2}(y)|}{u_2 - \dot{\psi}y}, \qquad t_2(y) \le \mu p$$

being k a (positive) proportionality factor between slip ratio and force per unit length. t_1 and t_2 are positive by definition and they are saturated with μp. This is a combination of a isotropic viscous friction model (related to k) and an isotropic Coulomb model (related to the saturation values for t_1 and t_2) [9].The denominator reflect the same idea presented in [7], i.e. it represents the velocity at which friction changes from static to dynamic. Based on classical tire/vehicle dynamics, such change takes place at slip ratios around 10-15%, therefore k is chosen as $k = \frac{\mu p}{0.15} \approx 2200$ N/m (for an average friction coefficient equal to 0.5). More complicated models might be adopted in a future implementation (e.g. [4]).

The longitudinal and lateral forces generated at each point of the contact line are

$$t_{x1}(y) = t_1(y)\frac{-\Delta V_{1x}(y)}{|\Delta \boldsymbol{V_1}(y)|},\ t_{y1}(y) = t_1(y)\frac{-\Delta V_{1y}}{|\Delta \boldsymbol{V_1}(y)|},$$
$$t_{x2}(y) = t_2(y)\frac{-\Delta V_{2x}(y)}{|\Delta \boldsymbol{V_2}(y)|},\ t_{y2}(y) = t_2(y)\frac{-\Delta V_{2y}}{|\Delta \boldsymbol{V_2}(y)|}$$

The overall longitudinal and lateral forces generated at each module are

$$Fx_1 = \int_{-b/2}^{b/2} t_{x1}(y)\ \mathrm{d}y,\ Fy_1 = \int_{-b/2}^{b/2} t_{y1}(\mathrm{y})\ \mathrm{d}y,$$
$$Fx_2 = \int_{-b/2}^{b/2} t_{x2}(y)\ \mathrm{d}y,\ Fy_2 = \int_{-b/2}^{b/2} t_{y2}(y)\ \mathrm{d}y$$

Finally, the moment arms Y_1 and Y_2 can be calculated as

$$Y_1 = -\frac{\int_{-b/2}^{b/2} t_{x1}(y)y\ \mathrm{d}y}{Fx_1},\ Y_2 = -\frac{\int_{-b/2}^{b/2} t_{x2}(y)y\ \mathrm{d}y}{Fx_2}$$

where the minus sign is due to the adopted sign convention (e.g., a force along axis $\boldsymbol{x_1}$ applied at a positive Y_1 produces a clockwise, i.e. negative, moment, that must be consistent with the convention adopted when writing the equilibrium

equations). Trajectories are calculated based on Eq. 3.9 from [6] and on the yaw angle covered by the robot, ψ, written in $\{S_1\}$ with initial value zero, $\psi = \int \dot{\psi}\, dt$.

The longitudinal and lateral position of the centre of mass are

$${}^1x = \int (u\cos\psi - v\sin\psi)\, dt\,,\quad {}^1y = \int (u\sin\psi + v\cos\psi)\, dt$$

with initial values $\frac{d}{2}(1-\cos\theta)$ for x, and $\frac{d}{2}\sin\theta$ for y.

The longitudinal and lateral position of the centre of mass of module 1 are

$${}^1x_1 = \int \left(\left(u + r\frac{d}{2}\sin\theta \right)\cos\psi - \left(v + r\frac{d}{2}(1+\cos\theta) \right)\sin\psi \right) dt$$

$${}^1y_1 = \int \left(\left(u + r\frac{d}{2}\sin\theta \right)\sin\psi + v + r\frac{d}{2}(1+\cos\theta)\cos\psi \right) dt$$

with initial value d for x_1, and zero for y_1.

The longitudinal and lateral position of the centre of mass of module 1 are

$${}^1x_2 = \int \left(\left(u\cos\theta - v\sin\theta + r\frac{d}{2}\sin\theta \right)\cos\psi - \left(u\sin\theta + v\cos\theta - r\frac{d}{2}(1+\cos\theta) \right)\sin\psi \right) dt$$

$${}^1y_2 = \int \left(\left(u\cos\theta - v\sin\theta + r\frac{d}{2}\sin\theta \right)\sin\psi + \left(u\sin\theta + v\cos\theta - r\frac{d}{2}(1+\cos\theta) \right)\cos\psi \right) dt$$

with initial values $-d\cos\vartheta$ for x_2, and $d\sin\vartheta$ for y_2.

Trajectory plots in the remainder are plotted in $\{S_1\}$. Due to the assumptions above, the trajectory of point O will originate from (0,0).

3 Results

A selection of results is presented in this section. In particular, the numerical value herein adopted are $m = 5$ kg, $R = 0.0525$ m, $d = 0.1875$ m. The vehicle is standstill at the beginning of the simulation, then it experiences a transient due to the roller angular velocities, and eventually it reaches a steady-state condition. The plots below are referred to the latter. Fig. 4 reports the steady-state curvature radius of the vehicle centre of mass as a function of the wheel tangential velocity, for two values of friction coefficient, 0.1 and 1. The steady-state curvature radius is not affected by the tangential velocity when this is relatively low. Yet, the steady-state yaw rate (not shown) is higher for higher tangential velocities of the rollers.

As the wheel angular velocity increases, at some point (depending on the friction coefficient) there is a significant drop of the curvature radius, e.g. around 32 rad/s for $\mu = 0.1$ and $\theta = 5°$. A visual representation of the forces generated right before and after such drop is reported in Fig. 5 and Fig. 6. Looking at Fig. 5, for relatively low angular velocities of the roller, each module reaches a steady-state forward velocity pretty similar to the relative tangential velocity of the roller, V_T^r (1.6 m/s in this case with $\omega = 30.5$ rad/s), hence the longitudinal sliding velocity is approximately zero around the centre of each module, and so is the longitudinal force. Due to the vehicle turning left, the inner (left) part of the module will have a velocity component towards the rear, hence the force generated will be directed towards the front of the module, and vice-versa for the outer part of the module (Fig. 5). However, when the angular velocity of the rollers is too high for the vehicle to achieve V_T^r ($\omega = 32$ rad/s in Fig. 6), due to the robot geometry (yaw angle) and the friction coefficient, the whole modules will be sliding towards the rear, generating a longitudinal force towards the front of the module, both for the inner and outer part of the module (Fig. 6). This generates an increased yaw moment with respect to centre of mass of the robot (which lies on the left of the modules in this example with positive θ, as in Fig. 2), provoking a decrease in the curvature radius. As the wheel tangential velocity keeps increasing, a combination of effects come into play, including force saturation and the distribution, explaining the increasing-decreasing behaviour of the curvature radius after the drop.

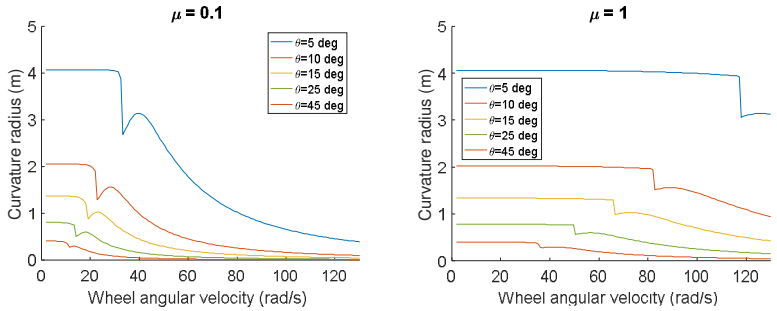

Fig. 4. Curvature radius as a function of wheel angular velocity ω and yaw angle θ, for two values of friction coefficient

Finally, Fig. 7 shows an example of vehicle trajectory for different values of θ, including the so-called kinematic trajectory i.e. the ideal trajectory covered in slip-free conditions. Interestingly, the robot exhibits a slightly understeering behaviour at the beginning of the simulation, whilst soon after it evolves into oversteer.

4 Conclusions

A simplified dynamic model for the snake robot Rese_Q01 was presented. The preliminary results are encouraging. They will be an helpful starting point for the

forthcoming mechanical design of the robot. As the project will progress, it is expected that more detailed analyses will be carried out, due to simplifying hypotheses being progressively dropped, e.g. number of rollers per module, number of modules, normal force distribution, and so forth.

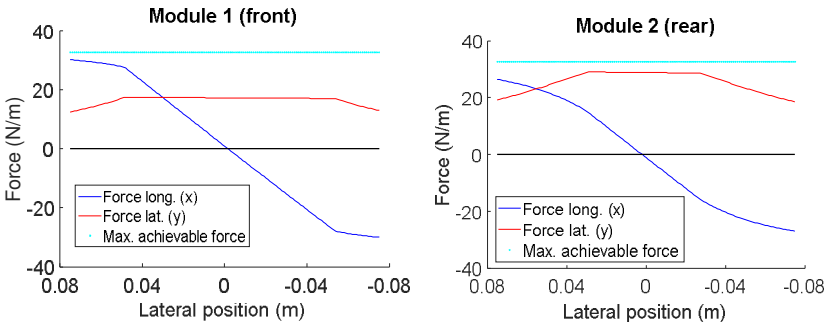

Fig. 5. Forces per unit length, front and rear module, $\omega = 30.5$ rad/s, $\mu = 0.1$

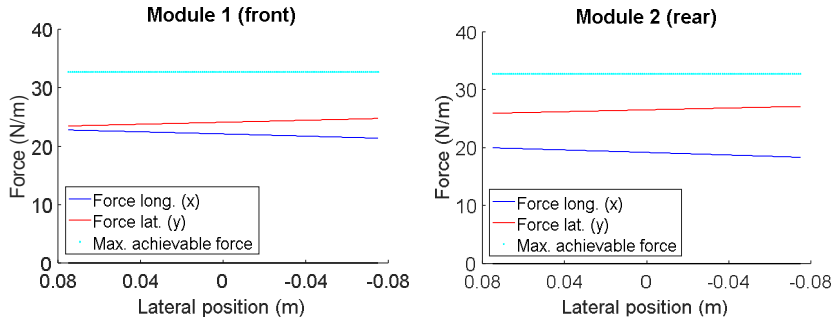

Fig. 6. Forces per unit length, front and rear module, $\omega = 36$ rad/s, $\mu = 0.1$

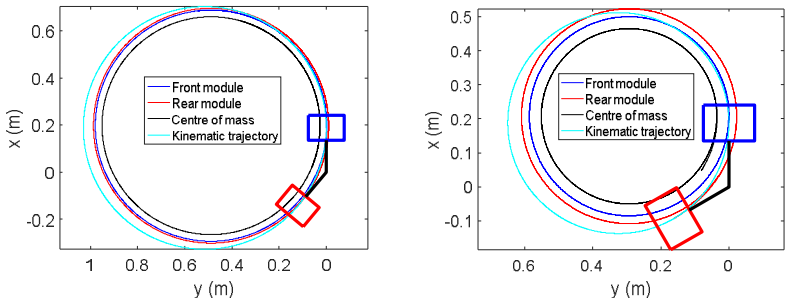

Fig. 7. Vehicle trajectory, robot depicted at initial conditions, $\omega = 7.7$ rad/s, $\mu = 0.1$, (left) $\theta = 40$ deg, (right) $\theta = 60$ deg

References

[1] https://ifr.org/, last accessed 21/06/2018.

[2] Adams, A.A., Charles, P.T., et al.: REMUS100 AUV with an integrated microfluidic system for explosives dectetion, Analytical and bioanalytical chemistry, 405:15, 5171-5178 (2013)

[3] Bruzzone, L., Quaglia, G., "Review article: locomotion systems for ground mobile robots in unstructured environments", Mechanical sciences, 3:2, 49-62 (2012)

[4] Calabrese, F., Farroni, F., Timpone, F.: A flexible ring tyre model for normal interaction, International Review on Modelling and Simulations (I.RE.MO.S.), Vol. 6, N. 4 (2013)

[5] De Filippis, G. Lenzo, B., Sorniotti, A., Gruber, P., De Nijs, W.: Energy-Efficient Torque-Vectoring Control of Electric Vehicles with Multiple Drivetrains, IEEE Transactions on Vehicular Technology, 67:6 (2018)

[6] Guiggiani, M.: The Science of Vehicle Dynamics, Springer (2014)

[7] Kalani, H., Akbarzadeh, A.: Effect of Friction Models on Snake Robot Performance, International Journal of Modeling and Optimization, 1:2, 129 (2011)

[8] Lenzo, B., De Filippis, G., Dizqah, A. M., Sorniotti, A., Gruber, P., Fallah, S., De Nijs, W.: Torque Distribution Strategies for Energy-Efficient Electric Vehicles with Multiple Drivetrains, ASME Journal of Dynamic Systems, Measurement and Control, 139:12 (2017)

[9] Liljebäck, P., Pettersen, K. Y., Stavdahl, Ø., Gravdahl, J. T.: Snake Robots, Springer London (2013)

[10] Nedjati, A., Vizvari, B., Izbirak, G.: Post earthquake response by small UAV helicopter, Natural Hazards, 80:3, 1669-1688 (2016)

[11] Qiao, G., et al.: A Wheel-legged Robot with Active Waist Joint: Design, Analysis, and Experimental Results", Journal of Intelligent & Robotic Systems, 83:3-4, 485-502 (2016)

[12] Quaglia, G., Nisi, M., Bruzzone, L., Fanghella, P.: Path Tracking Experimentation With Epi.q-Mod 2: An Obstacle Climbing Mobile Robot, ASME IMECE 2016 (2016)

[13] Quaglia, G., Cavallone, P.: Rese_Q: UGV for rescue tasks functional design, Accepted by Proceedings of the ASME 2018 IMECE (2018)

[14] Quaglia, G., Nisi, M.: Design of a self-leveling cam mechanism for a stair climbing wheelchair, Mechanism and Machine Theory, 112, 84-104 (2017)

[15] Quaglia, G., Franco W., Nisi M.: Design of a reconfiguration mechanism for an electric stair-climbing wheelchair, ASME IMECE2014 Int. Mech. Eng. Congress and Expo (2014)

[16] Quaglia, G., Cavallone, P., Visconte, C.: Agri_q: Agriculture UGV for Monitoring and Drone Landing, Accepted by MEDER 2018 Symposium (2018)

[17] Tota, A., et al.: On the experimental analysis of integral sliding modes for yaw rate and sideslip control of an electric vehicle with multiple motors. Int. J. of Autom. Tech. (2018)

[18] Wang, Z., Montanaro, U., Fallah, S. et. al.: A gain scheduled robust linear quadratic regulator for vehicle direct yaw moment Control. Mechatronics, 51, 31-45 (2018)

[19] Xuehe, Z., Ge, L., Gangfeng, L., Jie, Z., ZhenXiu, H.: GPU based real-time SLAM of six-legged robot, Microprocessors and Microsystems, 47, 104-111 (2016)

[20] Yang, B., Han, L., Li, G., Xu, W., Hu, B.: A modular amphibious snake-like robot: Design, Modeling and Simulation, Proceedings of the 2015 IEEE Conference on Robotics and Biomimetics, 1924-1929 (2015)